

A cloud model of active galactic nuclei: the iron $K\alpha$ line diagnostics

V. Karas,^{1*} B. Czerny,² A. Abrassart³ and M. A. Abramowicz⁴

¹*Astronomical Institute, Charles University Prague, V Holešovičkách 2, CZ-180 00 Praha, Czech Republic*

²*Nicolaus Copernicus Astronomical Center, Bartycka 18, PL-00 716 Warsaw, Poland*

³*DAEC, Observatoire de Paris, Section de Meudon, F-92 195 Meudon, France*

⁴*Institute for Theoretical Physics, Göteborg University and Chalmers University of Technology, S-412 96 Göteborg, Sweden*

Accepted 2000; Received 1999

ABSTRACT

The origin and the profile of the iron $K\alpha$ line from active galactic nuclei is being studied. The model with a quasi-spherical distribution of clouds around a compact galactic nucleus is explored in which the intrinsic spectral feature around 6–7 keV is substantially affected by Comptonization of primary X-rays. The predicted spectral profiles are influenced mainly by motion of the clouds in strong gravitational field of the centre, and by orientation of the source with respect to the observer. The case of the Seyfert galaxy MCG–6-30-15 is examined in more detail and free parameters of the model are determined. A robust result is obtained: acceptable fits to the observed profile correspond to the spherical distribution of the clouds with strong self-obscuration effects and with rather high value of ionization parameter. This is a different situation from that considered in the model of a cold illuminated disc. Nevertheless, geometrically flat (disc-type) configurations are not rejected.

Key words: Galaxies: active – Galaxies: Seyfert – X-rays: galaxies – X-rays: stars – Accretion, accretion discs – Galaxies: individual (MCG–6-30-15)

1 INTRODUCTION

An ever-increasing accuracy of the determination of the observed shape of the iron $K\alpha$ line in the Seyfert 1 galaxy MCG–6-30-15, and the evidence of the broad and skewed profile (Tanaka et al. 1995; Iwasawa et al. 1996) have led to wide acceptance of the model with an accreting black hole in the nucleus, and it offered an unprecedented opportunity to explore directly the pattern of the accretion flow onto the central hole in active galactic nuclei (AGN; for recent and detailed expositions of the subject, see Peterson 1997; Krolik 1999). The iron reflection features and remarkable variability patterns have been reported in many other AGN, galactic black-hole candidates, and similar objects.

It is the main aim of the present paper to examine relationship between the form of motion of the gaseous material in a galactic nucleus and the resulting profile of the spectral features. We concentrate ourselves on the question whether current observational evidence can be explained in terms of individual clouds with spherical or almost spherical (rather than disc-type) orbital motion around the centre, or

if strongly flattened distribution of the clouds is preferred resembling a disc or a ring (different models of the line formation in AGN were reviewed by Netzer 1990). This topic has far-reaching consequences for the unification scheme of AGN (Antonucci 1993). Although the assumptions of the disc geometry and of strictly planar bulk motion of the gaseous material are relaxed in the present paper, the presence of a compact supermassive accreting nucleus remains crucial for explaining the observed spectral features.

Broad iron features were expected in X-ray spectra on the basis of the model in which the iron line is formed on the surface of a geometrically thin, optically thick and relatively cold medium after irradiation by a primary source (Fabian et al. 1989). Subsequent detailed fits to observational data confirmed that the line profile is in agreement with the predictions of the accretion disc model in which the intrinsically narrow line, emitted at energy 6.4 keV, is gravitationally shifted and Doppler broadened/boosted due to the disc orbital motion. Comparisons of the model with the data allow one to constrain the disc inclination angle, the range of disc radii contributing to the emission, and the radial dependence of the incident X-ray flux, although there are various uncertainties if astrophysically more realistic models of accretion flows are introduced, and if the lack of resolution and the noise in available data are taken

* E-mail: vladimir.karas@mff.cuni.cz (VK); bcz@camk.edu.pl (BC); arnaud.abrassart@obspm.fr (AA); marek@fy.chalmers.se (MAA)

into account; cf. Fabian et al. (1989); Tanaka et al. (1995); Weaver & Reynolds (1998) for the case of iron line diagnostics, and Rokaki & Boisson (1999) for application to UV continuum and $H\beta$ emission line.

The expected amplitude of the line profiles and the characteristic form of continuum from X-ray illuminated accretion flows were examined, taking into account combination of effects due to high orbital velocities and strong gravity near the nucleus (George & Fabian 1991; Matt, Perola & Stella 1993). It has been argued with various levels of refinement that parameters of the central black hole (especially its angular momentum) can be inferred from disc-line spectra, assuming that they are sensitive to the radius of the innermost stable orbit whose imprint is visible in radiation of the accretion flow (Laor 1991; Iwasawa et al. 1996; Dabrowski et al. 1997; Pariev & Bromley 1998).

Reynolds & Begelman (1997) pointed out, however, that the model is not that sensitive to the value of the spin of the hole if the contribution to the line is allowed also from matter inspiralling below the marginally stable orbit, r_{ms} . Such a possibility appears as perfectly consistent with high efficiency of X-ray radiation if the adopted geometrical depth of the stream is small, in agreement with actual computations of the flow properties below r_{ms} (Muchotrzeb & Paczyński 1982).

In the case of accretion-disc geometry, and with different assumptions about the X-ray illumination and reprocessing, the predicted spectra (line plus continuum) have been calculated by several authors (recently Young, Ross & Fabian 1998; Martocchia, Karas & Matt 2000; see further references therein). The same scheme, coupling the shape and the amplitude of the line with the shape and the amplitude of the Compton reflection component, was successfully applied to galactic black-hole candidates (Życki, Done & Smith 1998; Done & Życki 1999).

The line fits are consistent with the line emitted at intrinsic energy 6.4 keV (so it comes from weakly ionized iron) while the broad shape of the spectral feature indicates that it is formed near the innermost part of the disc, following intense irradiation. This might be related to the specific slope of the hard X-ray emission (Rózańska et al. 2000; Nayakshin, Kazanas & Kallman 1999). The blue wing of the line is in all sources linked with the broad feature around 6.4 keV, requiring somewhat special interplay between model parameters. Namely, strong constraints are imposed on the inclination angle of the disc [see Guainazzi et al. (1999) for the case of MCG-6-30-15; Wang, Zhou & Wang (1999) for NGC 4151; Nandra et al. (1999) for NGC 3516] although contribution to the total light from various components helps to ease this constraint to some extent.

Sulentic et al. (1998b) raised the problem of disagreement between the inclination angle derived by two independent approaches: from the iron-line model, and from $H\beta$ and $H\alpha$ measurements. In a large sample of objects, the position of the line centroid at 6.4 keV is not consistent with the random orientation of the disc with respect to the observer (Sulentic, Marziani & Calvani 1998a) although this problem is weakened by the fact that the Balmer lines do not necessarily have to come from the outer parts of the disc, as assumed in the paper. In particular, the mean inclination derived for a sample of Seyfert 2 galaxies does not differ from the mean inclination angle of Seyfert 1 galaxies (Turner et

al. 1998), which disagrees with the widely preferred unification scheme (however, see Weaver & Reynolds 1998). Also, the outer disc radius comes out lowish, of the order of ten Schwarzschild radii ($r_s \doteq 2.95 \times 10^5 M/M_\odot$ cm in terms of the central black-hole mass M). The problem of this apparent disagreement in inclination angles can be weakened by the fact that the Balmer lines do not necessarily have to come from the outer parts of the disc, as assumed in the paper, and there is also a contribution from the narrow unresolved component (expected to arise in the dusty/molecular torus; Krolik, Madau & Życki 1994) which has not been properly accounted.

Certain doubts concerning the disc model for the iron-line production revived the interest in the alternative explanation of the line profile (Czerny, Zbyszewska & Raine 1991). Misra & Sutarra (1999) assume that the line is produced by Compton scattering of the line photons in warm, Thomson thick material. They show that such a model fits the data equally well as the disc model, but the approach may look rather ad hoc because the origin and location of the Comptonizing medium have not been addressed in their paper, neither the source of the X/UV incident continuum that is a necessary ingredient of this model. A better motivated approach was adopted by Abrassart (2000a; see further references cited therein) who explored spectral properties within the frame of the clouds model of accretion onto a black hole where both the line formation and Comptonization occur in the same medium. However, his results did not incorporate the global effects (gravitational redshift, clouds motion, etc). Hereafter we will argue that these effects cannot be ignored.

In the present paper we discuss the possibility of explaining the Fe $K\alpha$ line within the frame of the model in which the innermost part of the disc is disrupted due to disc instabilities. Part of the disc material forms optically thick cold clouds, while another fraction heats up to high temperatures acting as a source of X-rays. The clouds are not confined to the disc equatorial plane, and they form a layer covering a significant portion of the sky from the point of view of the central X-ray source (Collin-Souffrin et al. 1996). In this model the line profiles are determined by two concurrent effects: they arise partially from the Comptonization within the material significantly ionized at the surface of the clouds (the intrinsic line profile), and partially from kinematics of the clouds distribution and from strength of the gravitational field where the clouds persist (smearing of the profile). In the next section we formulate a simplified model which captures the essence of the clouds scenario and can be further developed to a more realistic form. We show the predicted line profiles as a function of model parameters (specified by the clouds distribution) and the observer view angle. The intrinsic shape of the spectral feature has been taken either as a narrow delta-type line, or a numerically computed broad feature (corresponding to high ionization parameter ξ). Then we briefly discuss how various complications (obscuration of the clouds, non-Keplerian orbital motion) are reflected in resulting profiles (Sec. 3). We conclude the paper by comparison with the *ASCA* data for MCG-6-30-15, and we discuss overall advantages and the problems of this picture.

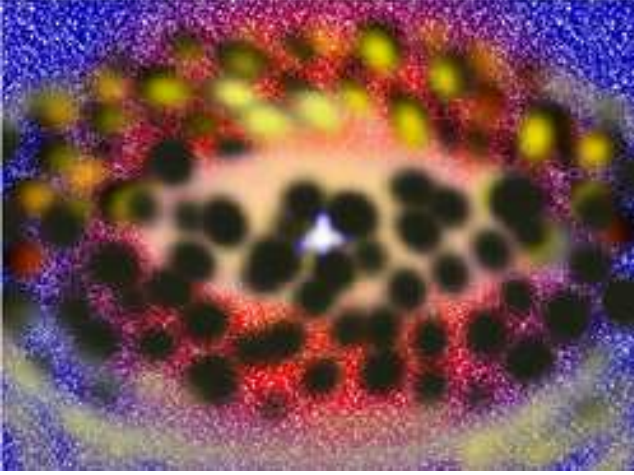


Figure 1. A schematic view showing the main ingredients of the model. Most of the clouds are distributed at some characteristic radius, their origin being presumably in the accretion disc disrupted due to instabilities. The clouds survive as individual entities orbiting around the massive and compact core. They are irradiated from the centre, and the primary X-rays are reprocessed on the clouds surfaces. From the observer's view, dark parts of the clouds are in front of the nucleus while radiating surfaces correspond to the clouds in the back side. The intrinsic spectrum is determined mainly by the Comptonization, depending sensitively on ionization parameter. Rather clean line of sight to the central source emerges among the clouds. The observed spectral features are then influenced by the clouds distribution, their velocities, and self-obscuration effects. Also the aspect angle of the observer must be considered if the distribution is flattened rather than spherically symmetric.

2 THE MODEL

We assume that the iron $K\alpha$ line is produced by irradiated surfaces of the clouds. The clouds could be formed from the inner accretion disc which is eroded at a distance of a few or a few tens of Schwarzschild radii. The basic principles of the model were outlined by Collin-Souffrin et al. (1996), and the broad-band spectra following from this model were studied by Czerny & Dumont (1998). The expected shape of $K\alpha$ line was calculated with careful consideration of X-ray reprocessing (Abrassart 2000b) but without taking into account any kinematical and gravitational effects which must influence the observed spectral features substantially if the clouds are to be located so close to the central black hole. Resulting width and centroid energy of the line were thus entirely due to the Comptonization. In those papers, the clouds distribution was assumed to be spherical and positions of all the clouds were fixed at a given distance from the black hole.

Here, we relax the assumption of stationary clouds forming a spherical layer with strictly uniform distribution. Instead, the clouds follow planar orbits departing from the equatorial plane of the disc (Figure 1). One of the appealing advantages of this scheme is the naturally modeled variability of X-ray sources due to obscuration events (Abrassart & Czerny 2000). In the present paper it is assumed that excursions of the clouds from equatorial plane are limited by the maximum angle of deflection, say θ_m . This angle, and radius of the clouds belt, r , stand as two free parameters in the simplest version of the model. The assumed distribution

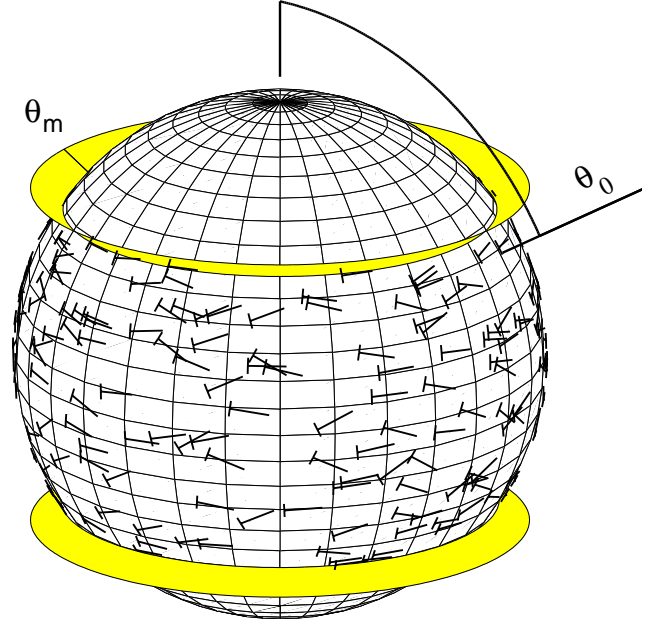


Figure 2. A representation of the clouds distribution (positions and velocities of the clouds). In this sketch we consider all the clouds being located on the surface of a sphere. Their trajectories are characterized by constant value of the radius r , and by maximum excursion θ_m from the equatorial plane. The clouds are distributed randomly within the allowed range of latitude which also restricts directions of the clouds velocities (indicated by short dashes). Observer's inclination angle θ_0 is also shown.

accommodates both the case developed by Collin-Souffrin et al. (1996), and the case of a narrow ring (Gerbal & Pelat 1981) in the limiting values of θ_m . In principle, our model can accommodate a system of clouds on both prograde and retrograde orbits with respect to the disc, but an intermediate value of the clouds departure from the equatorial plane appears as most favourable, corresponding to quasi-spherical or somewhat flattened system of the clouds following more or less corotating trajectories. This case allows for quite high covering factor (necessary in the model which relies on multiple scattering of radiation among the clouds) while reducing the rate of collisions (which otherwise tend to destroy the clouds).

The present model does not require all the individual clouds to preserve their identity for many orbital periods or even indefinitely. Although it may appear easier in this scheme to think of the clouds as separate entities, the predicted spectrum will not change if the clouds have a finite and very limited lifetime, assuming they are continuously replaced by newly created ones. Each of the clouds can be removed from the system after, say, one revolution, either due to collisional destruction with other clouds or by heating up to the state when it does not contribute to the line spectrum and possibly evaporates. In the other words, the spectral features would be expected more pronounced during the initial phase of the cloud's history before reaching the equilibrium.

Radiation of the clouds surface is characterized by intrinsic emissivity which is assumed constant and isotropical in the local comoving (rest) frame of each cloud. Since the distribution is not spherically symmetric in general, the

observed spectrum depends on inclination angle of the observer. We neglect the contribution to the line coming possibly from the outer, fairly smooth part of the disc. The intrinsic line profiles of the clouds come out somewhat different from those which are usually adopted in the disc-line model (cf. Sec. 3), and the random motion of the clouds must be also taken into account in calculations of predicted spectra.

2.1 Kinematical and gravitational effects

The basic observational properties relevant for this paper, i.e. the observed profiles of spectral features (their centroid energies and widths in particular), can be roughly predicted by a simplified model in which the clouds distribution is specified by a small number of phenomenological parameters. Notice, however, that one still needs to solve for the radiation reprocessing in order to obtain the intrinsic line profiles.

In the simplest version of the model, the observer is located at inclination θ_0 far from the source ($0 \leq \theta_0 \leq \pi/2$), while all the clouds are distributed at the same radial distance and they move with the corresponding Keplerian orbital velocity, $v_k(r)$. Gravitational field of the central body is spherically symmetric and described by the Newton law. We introduce Schwarzschild radius $r_s = 2GM/c^2$ as a convenient length-scale and we use geometrized units with $G = c = 1$ hereafter.

The clouds are distributed randomly within a band of spherical latitudes: $\pi/2 - \theta_m \leq \theta \leq \pi/2 + \theta_m$ (Figure 2). Spherical coordinates r, θ, ϕ are employed with the disc plane at $\theta = \pi/2$. Parameter θ_m reflects the dynamics of the process of clouds formation and of their interaction with surrounding environment. If the disc disruption proceeds rapidly, and if the newly formed clouds are efficiently captured by some outflowing plasma and/or accelerated by the radiation pressure, then the clouds distribution can be approximately characterized by $r = \text{const}$ with relatively large θ_m . On the other hand, if the clouds acceleration is only moderate in the direction perpendicular to the disc plane, and if their subsequent evaporation is fast in comparison with the timescale of latitudinal motion, then the distribution is again well characterized by constant radius but rather small θ_m .

Velocity of the clouds points along $r = \text{const}$ surface and its direction defines the angle α :

$$\mathbf{v} = v_k(\cos \alpha \mathbf{e}_\phi - \sin \alpha \mathbf{e}_\theta). \quad (1)$$

The range of possible values of α is determined by the angular width θ_m of the clouds distribution. Straightforward trigonometry gives relation for the maximum α of the clouds velocities,

$$\begin{aligned} \sin \alpha &= \pm (\cos \theta \cot \theta \cot \theta_m \cos \theta_m - \sin \theta \sin \theta_m) \\ &\times (1 - \cos^2 \theta \sin^{-2} \theta_m)^{1/2} \\ &\mp \cos^2 \theta \sin^{-1} \theta_m (1 - \cot^2 \theta \cot^2 \theta_m)^{1/2}. \end{aligned} \quad (2)$$

This relation is shown in Figure 3 where θ_m stands as parameter of the curves $\alpha(\theta; \theta_m)$. For example: one can read in the graph that latitudinal motion of the clouds has turning points at $\alpha(\pi/2 - \theta_m; \theta_m) = 0$ where trajectories are parallel to the disc plane (i.e. $\mathbf{v} \parallel \mathbf{e}_\phi$). The upper/lower signs in

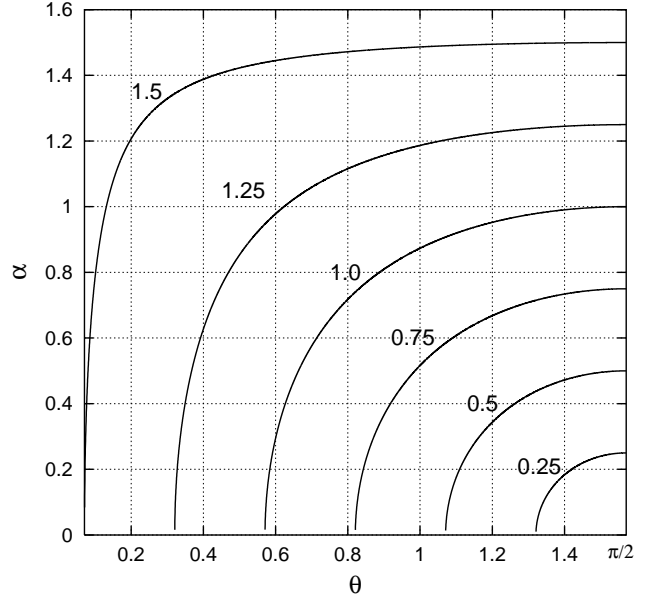


Figure 3. The range of allowed values of angle α constraining the velocity direction of the clouds as a function of θ [cf. eq. (1)]. The curves are labeled with the corresponding latitudinal boundary θ_m of the clouds belt, which adopts values from $\theta_m = \pi/2$ (strictly spherical distribution) down to $\theta_m = 0$ (the equatorial ring).

eq. (2) correspond to the descending/ascending parts of the trajectory, respectively. We recall that for $\theta_m \rightarrow 0$ the clouds remain in the equatorial plane (ring-like distribution), while for $\theta_m = \pi/2$ the clouds are spread uniformly over the whole sphere (with random distribution).

The observed radiation of a cloud is determined by special-relativity effects which influence photon energy E and intensity $I(E)$ in usual manner (Cunningham & Bardeen 1973): $I(E) = I_e(E/g)g^3$ where I_e is the emitted intensity, and g is the redshift factor defining the change of energy. We adopt standard notation, similar to Ohna et al. (1995) who studied a related problem with application to fast winds. In our case, however, it is the inner part of the clouds surfaces which is hot enough to emit the X-rays. The remote part of the clouds (with respect to the central source) is not subject to primary irradiation, and it emits almost no X-rays at all. As a consequence of self-obscurtion, X-rays are visible only from the clouds with appropriate orientation, and their radiating area is further reduced on the rim of the image by projection effect. In addition, mutual eclipses of the clouds must be considered. The resulting obscuration is enhanced in the case of clouds which substantially overlap each other; we will characterize this effect by another free parameter $[\omega]$; cf. eq. (4) below].

2.1.1 The case of negligible obscuration

First we ignore entirely the obscuration of the clouds by other clouds. We assume that the clouds radiate isotropically in their local comoving frame, and they are of spherical shape with an infinitesimally small radius (i.e. much less than r_s). In this case all the clouds from the whole hemisphere contribute to observed X-rays.

The redshift factor g depends on the angle between ve-

locity of the cloud and the unit vector \mathbf{s} towards the observer,

$$g = L^{-1} \gamma (1 - \mathbf{v} \cdot \mathbf{s}). \quad (3)$$

Here, $\gamma = 1/\sqrt{1-v^2}$ is the Lorentz factor, and $\mathbf{v} \cdot \mathbf{s} = v_k \cos \theta_0 \sin \alpha \sin \theta - v_k \sin \theta_0 (\cos \alpha \sin \phi + \sin \alpha \cos \theta \cos \phi)$. Integration of light over the clouds distribution yields the total observed radiation flux. Effects of general relativity are accounted by the gravitational redshift term $L = \sqrt{1 - r_s/r}$, but gravitational lensing has been ignored here for simplification (this might have some effect on the light from clouds at the upper conjunction).

Since we deal with the clouds that are irradiated by the central source, one expects the local emissivity to be depending on the angle between the direction towards center and the normal to the cloud's surface. In such a case, by a simple geometrical argument, the observed line profile of the whole axisymmetric collection of the clouds is the same as for the case of clouds radiating truly isotropically. This conclusion does not hold, however, if partial and non-axisymmetric self-obscuration of the clouds is involved.

2.1.2 Partial obscuration of the clouds

The presence of a large number of clouds (typically $N \approx 10^3$) enhances the chance of mutual obscuration among them. This effect cannot be ignored in this model because the observer receives X-rays only from those parts of the clouds which are on the inner side of the $r = \text{const}$ surface, and not too close to the edge of the image (as projected onto the observer image plane). It can be included in the model by introducing another parameter, say ω , characterizing the maximum angle between the line of sight and the edge of the clouds distribution: $\mathbf{s} \cdot \mathbf{e}_r = \cos(\pi - \omega)$. In other words, outgoing rays must pass from interior hot surfaces of the clouds through empty holes in between them before they can finally escape towards the observer. This is impossible near the projected rim of the sphere. Therefore in calculations of the observed radiation, only those clouds are considered which, in addition to the conditions described in the previous paragraph, satisfy also relation (Figure 4)

$$\sin \theta_0 \sin \theta \cos \phi + \cos \theta_0 \cos \theta > -\cos \omega. \quad (4)$$

Let us remark that the angle ω can be related to the covering factor f_c (defined as the fractional area of the sky subtended by the clouds as viewed from the centre of the source). The covering factor f_c can be expressed in terms of the clouds typical diameter d , typical distance l between the clouds, and their number N : $f_c = N(d/r)^2$, with the obscuration constraint $d \approx l \cos \omega$ for spherical clouds filling the whole $r = \text{const}$ surface (f_c obviously decreases with θ_m decreasing). The exact description of obscuration would require a specification of the clouds shapes, and it can be carried out only numerically by generating random clouds distributions with the constraints imposed by the visibility conditions, checking the line of sight in each case. Furthermore, d and l are linked to each other via N , but parameter ω has direct geometrical meaning in our model, and it appears thus convenient for the present discussion. In principle, the same value of the phenomenological parameter ω can correspond to different physical models of the clouds origin, their geometrical configuration and other details.

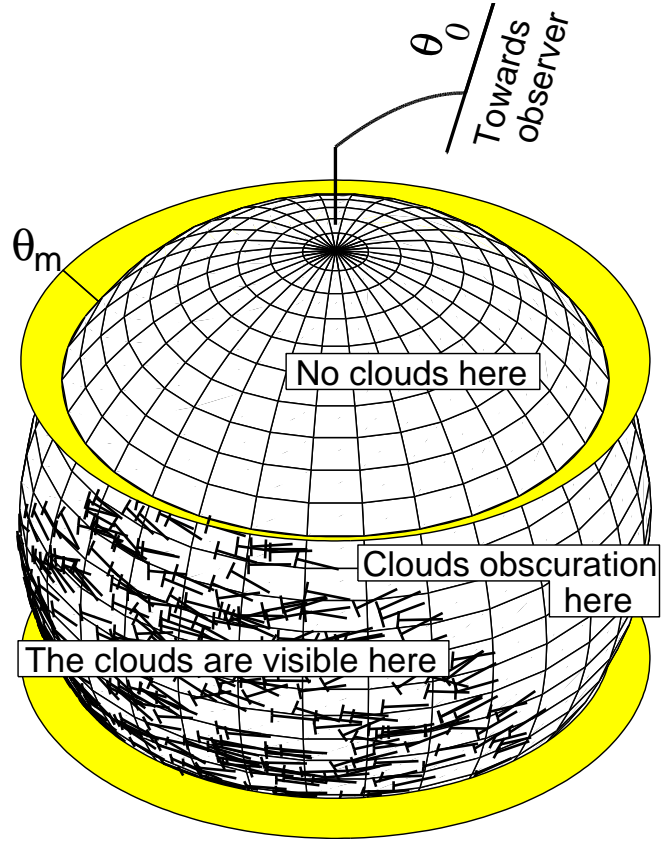


Figure 4. A view of the clouds distribution in the case of non-negligible obscuration. Positions and velocities of those clouds are shown which fulfil conditions of visibility (4). In comparison with Fig. 2, only a fraction of the clouds contribute to the observed spectrum: those moving more or less perpendicularly to the observer's line of sight. Direction towards the observer is shown with inclination angle θ_0 . Different regions are indicated on the sphere according to visibility of the clouds. The clouds do not reach high latitudes, and they enter in dead angle near the rim of the projected image. This figure corresponds to parameters $\theta_m = 30^\circ$, $\theta_0 = 60^\circ$, $\omega = 60^\circ$ in our notation.

2.2 The intrinsic line profile

The intrinsic shape of the iron line has been computed using a Monte Carlo code NOAR (Abrassart 2000b), coupled with the code TITAN (Dumont, Abrassart & Collin 2000) computing the ionization state of the gas for the assumed value of ionization parameter $\xi \equiv F_x/n$ (F_x denotes the incident X-ray flux, n is average number density of a cloud). The code TITAN serves to compute the radiative transfer in the Compton thick medium in a broad-band frequency range, and it includes the computations of opacity and temperature structure. It also gives local emissivity of the gas in various components of the $K\alpha$ line. The NOAR code uses the resulting opacity, it computes, in more detail, the transfer of hard X-ray photons, and provides better description of the details of hard X-ray spectra including Comptonization of the line within the hot surface layers of the clouds. It also describes the energy deposit by hard X-ray Compton heating for TITAN. The two codes are thus coupled and they both together offer the most accurate description of the iron line emission from the irradiated medium, assuming it is optically thick for electron scattering.

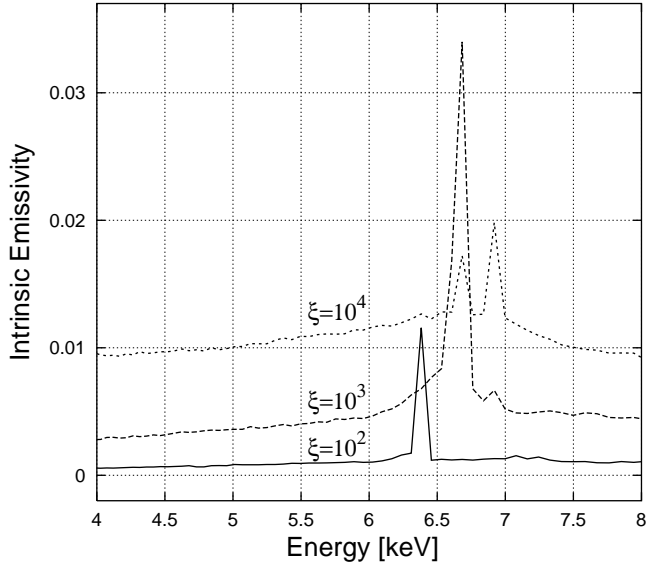


Figure 5. The intrinsic emissivity profile (arbitrary units) around the 6–7 keV spectral feature, as predicted by the Comptonization model for hot parts of the clouds surfaces. The three curves correspond to different values of the ionization parameter ξ (Abrassart 2000b).

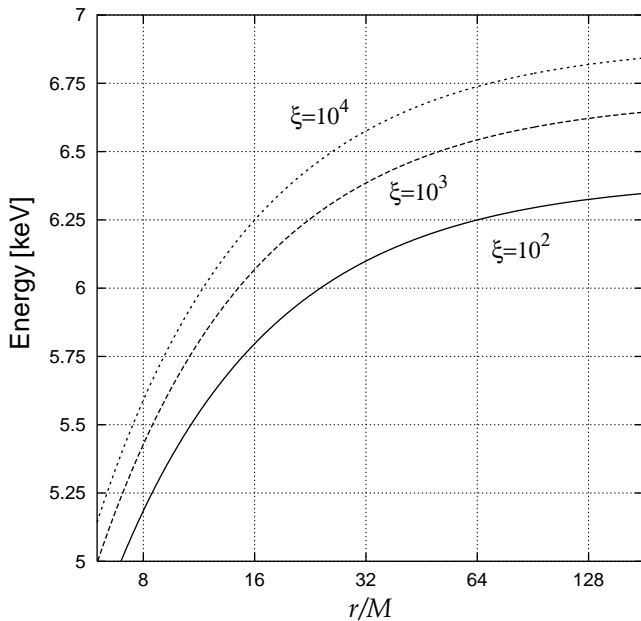


Figure 6. Relation between radius (logarithmic scale) and centroid energy of the line features dominating the intrinsic spectrum, after multiplication by that part of the redshift factor from eq. (3) which depends on r only and causes the overall redshift of the line. These curves correspond to the same values of ξ as in Fig. 5.

The computations were performed for a plane parallel slab corresponding to a sphere with large radius, so that multiple reflections between the clouds were neglected (they can effectively change only the value of the ionization parameter). The line profiles used in our computations of the cloud model are shown in Figure 5. The pattern obtained for $\xi = 10^2$ is centered at 6.4 keV, and it is so narrow that the

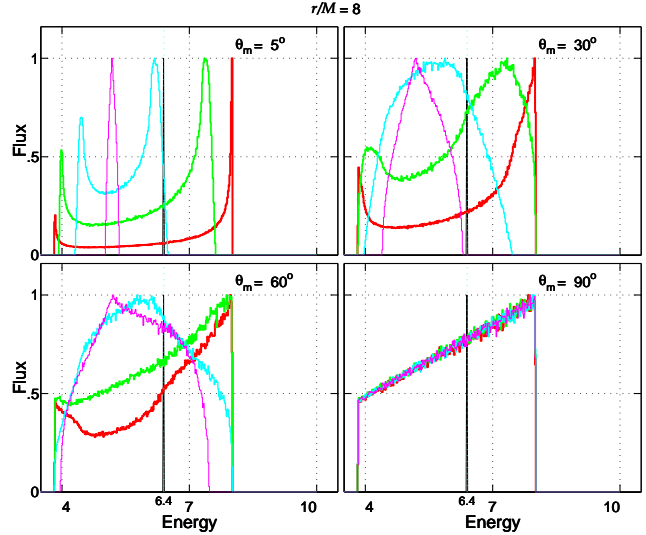


Figure 7. The expected line profile produced by the clouds sphere with $r = 8M$. The intrinsic emissivity has been assumed as a delta line at 6.4 keV. The four panels correspond to different angular widths of the clouds belt: $\theta_m = 5^\circ$ (almost equatorial ring), 30° , 60° , and 90° (strictly spherical distribution). In each panel, four curves correspond to different values of the observer inclination: $\theta_0 = 0$ (pole-on view, therefore the narrowest profile), 30° , 60° , 90° (equator-on view, the broadest profile). No obscuration is involved here. See the text for details.

line comes out almost unresolved, and any smaller degree of ionization would result in even narrower line. The line for $\xi = 10^3$ shows the peak shifted to 6.7 keV, and a broad red wing. The line for $\xi = 10^4$ contains a strong contribution of 6.9 keV component arising from hydrogen-like atoms; its red wing is extremely broad for such a high value of ionization.

Since the numerical computations of intrinsic profiles are exceedingly time consuming, we detach the line from its underlying reflected continuum and discuss the line spectrum separately. Such a simplification is possible because the line is not very sensitive to the slope of the incident X-ray radiation, while the reflected continuum depends on the slope considerably and would require computations of a set of different incident continuum slopes.

Figure 6 shows how the intrinsic centroid energy of the line is moved towards lower energy by factor $L(r) \gamma^{-1}(v_k(r))$ in eq. (3). This term is function of radius only. Therefore the graph shows roughly the mean energy of the expected observed line peaks from Fig. 5 depending on the radius of the clouds sphere.

In the next section we calculate the expected profiles for different parameters of the model. In particular, we further discuss the effect of broadening of the line, which arises from ϕ -dependent term $v \cdot s$ in eq. (3) and results in large equivalent widths and double-horn profiles in some cases.

3 RESULTS

3.1 A narrow intrinsic line

The computations performed with the codes TITAN and NOAR gave the Fe K α line strong but practically unresolved for the case of ionization parameter $\xi = 100$ under the

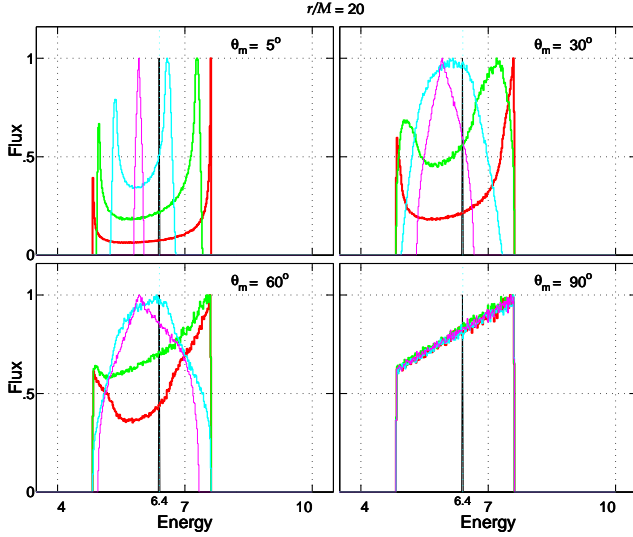


Figure 8. The same as in Fig. 7 but for $r = 20M$. Such intrinsically narrow profiles are expected in the case of low ionization of the clouds. They can also serve as templates for convolution with broader and more complex intrinsic profiles from a highly ionized medium.

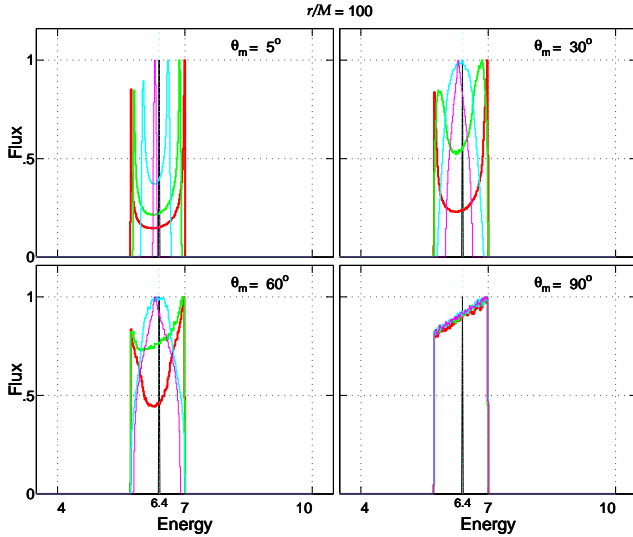


Figure 9. The same as in Fig. 7 but for $r = 100M$.

adopted energy grid: $\Delta E \approx 0.07 \text{ keV}$, and $\Delta E/E \approx 0.01$. A faint red wing is barely visible and it contains less than a few per cent of the line flux. Therefore, in order to study the case of a neutral iron line we could neglect the intrinsic width of the line and we performed computations assuming that all photons were emitted with energy 6.4 keV (delta-type line with no continuum background). The observed line profile is thus determined exclusively by radius of the clouds distribution r , the level of departure of the clouds from the equatorial plane θ_m , observer's angle θ_0 , and the obscuration parameter ω which is further related to the covering factor.

We show the predicted profiles for three different radii r of the clouds distributions (Figures 7–9). If the clouds occupy a very narrow belt on the sphere ($\theta_m \lesssim 5^\circ$), the resulting profiles are reduced to those obtained for a single

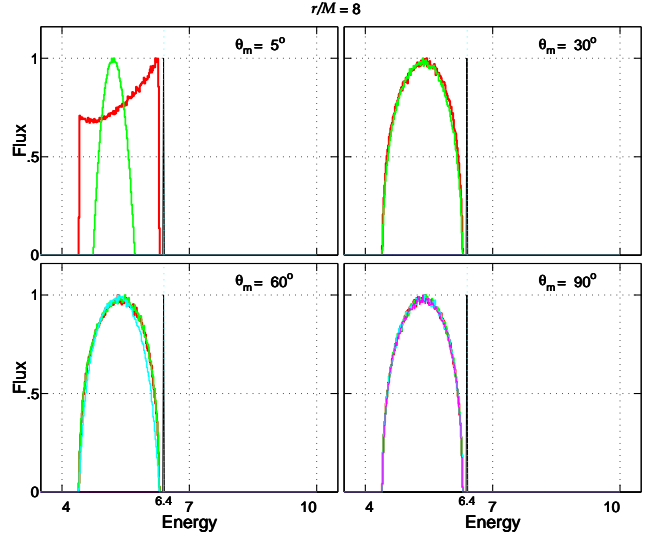


Figure 10. The predicted spectral profiles corresponding to delta-type line as in Fig. 7, but now the obscuration parameter has been introduced with $\omega = 30^\circ$. The dependence of the profiles on observer's inclination is substantially reduced in comparison with the previous case of negligible obscuration. Here, $r = 8M$.

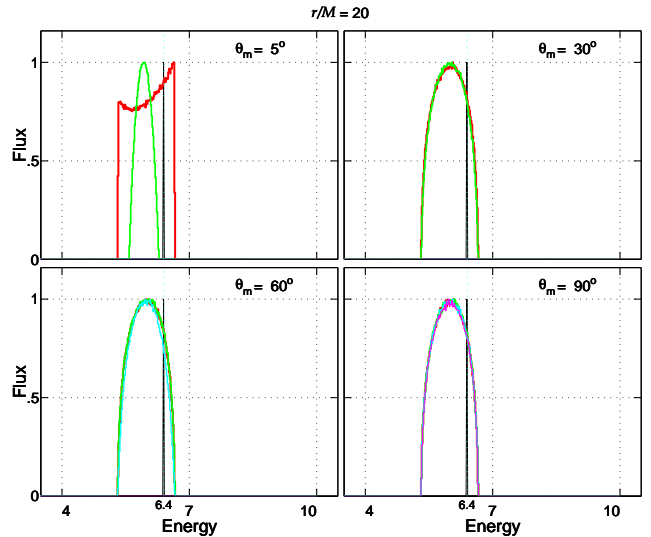


Figure 11. The same as in Fig. 10 but for $r = 20M$.

ring within the frame of the disc model of the line formation (Gerbal & Pelat 1981; Laor 1991). The corresponding values of r and θ_m are given on top of each figure. Two horns of the line are clearly seen with unequal heights due to the Doppler effect. The dependence of the profiles on θ_0 gets gradually diminished with increasing sphericity of the clouds distribution, as can be checked by comparing four panels with different θ_m . The profiles are normalized to the maximum flux.

Figs. 7–9 correspond to zero obscuration of the clouds ($\omega = 90^\circ$); the clouds do not shield each other and they all are seen by the observer. We remark that the resulting profiles are not completely smooth in these graphs because they are produced by individual sources of light. Naturally, the curves would appear very wiggly if the number of clouds

and the corresponding covering factor were small, but our simulations indicate quite large covering factors.

The resulting line profiles come out substantially different from the previous case of zero obscuration if $\omega \ll \pi/2$: the profiles get narrower, and they lose, partly or even completely, their double-horn shapes, so characteristic for ring-type sources (Figures 10–11). Considered jointly with the underlying continuum, there is less power in the line, so that equivalent width is diminished. The dependence on observer's inclination is further reduced by obscuration. One can easily deduce that the profiles do not depend on θ_0 if ω is small enough: $\omega \leq \theta_0 + \theta_m - \pi/2$. Also, notice that the constraints on the clouds visibility are not satisfied in case of very small θ_0 , ω and θ_m , so that the curves are shown only for appropriate combinations of these parameters.

What remains for the next section is to complete the above discussion by computing the expected profiles of more complicated intrinsic emissivities.

3.2 A broad intrinsic line

Now we examine the spectral features with intrinsically broad profiles and high ionization parameter ($\xi \gtrsim 10^3$; Abrassart 2000b). In each case the continuum had been fitted by a power-law outside the feature (4–9 keV), and then the result was subtracted from the predicted spectrum. In this way the expected spectral features have been obtained (Figures 12–13). We recall that the full (line and continuum) intrinsic spectra are the result of radiation transfer around 6.4 keV with multiple scattering among the clouds; they differ substantially from those corresponding to simple delta-line profiles. Here we present narrow band spectra; the actual energy range is shown on abscissae. The two figures differ by obscuration parameter ω : obscuration was ignored in the former, while it was assumed to be very large in the latter case.

Let us note that the values of f_c inferred from spectra fitting procedures (and corresponding parameter ω of the model) represent limiting boundary estimates of these quantities. One of the reasons of uncertainty is the clouds velocity which until now has been assumed fixed and equal to $v_k(r)$ while, in case of strong radiation pressure, the clouds motion may be non-Keplerian. The layer of clouds can be partially supported by intercepted radiation flux coming mainly from the center, so that steady-state motion of the clouds becomes sub-Keplerian. Therefore, given the observed line width, the actual covering factor will be less than that required on the basis of clouds free orbital motion. In the case of quasi-spherical distribution, the effect of radiation pressure is maximal for Eddington-type equilibrium condition, $GMm_p = \lambda$, where m_p is the proton mass, and

$$\lambda = \frac{L\sigma_T}{4\pi(1-f_c)c} \quad (5)$$

is the outward-directed radiation support due to total luminosity L corrected for partial obscuration. For large covering factor the total luminosity is small ($f_c \rightarrow 1$, $L \rightarrow 0$) and the ratio on the right-hand side of eq. (5) remains finite. Centroid energy of the line from such a static system of the clouds is determined by the intrinsic spectrum and gravitational redshift only, and the observed line width is reduced to the intrinsic one.

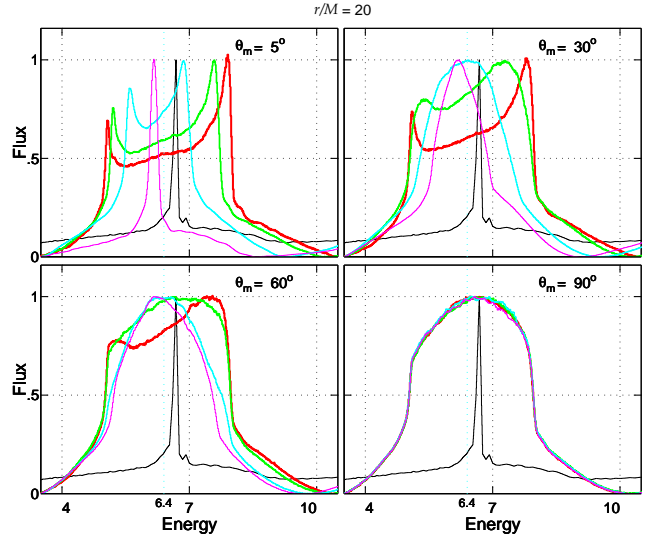


Figure 12. The expected iron-line profiles (power-law continuum subtracted) produced by the clouds at $r = 20M$ for four values of the inclination angle of observation θ_0 (0° , 30° , 60° , 90°). Again, the panels are labeled with the adopted values of the width of the belt, θ_m . The angle $\omega = 90^\circ$ corresponds to zero obscuration factor. The intrinsic spectrum is also plotted with the maximum at 6.7 keV, corresponding to the assumed ionization parameter, $\xi = 10^3$.

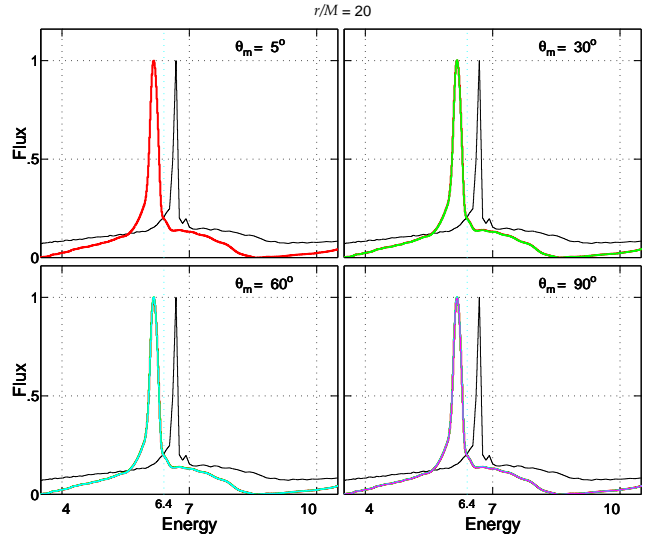


Figure 13. The same as in Fig. 12 but for $\omega = 10^\circ$.

3.3 The case of MCG–6-30-15

The Seyfert 1 galaxy MCG–6-30-15 is a notable example in which the extensive observational material has been collected. It shows the primary spectral slope of $\Gamma \approx 2.00 \pm 0.05$, as determined on the basis of joint *ASCA*/*RXTE* observations lasting ≈ 400 ksec with the cutoff energy at ≈ 100 keV (Lee et al. 1999). The disc-line scheme has been rather successful also for this object (Tanaka et al. 1995) and the conclusions drawn from the *ASCA* data are in agreement with the analysis based on *BeppoSAX* observations (Guainazzi et al. 1999). As a consequence, strong limits can be imposed on

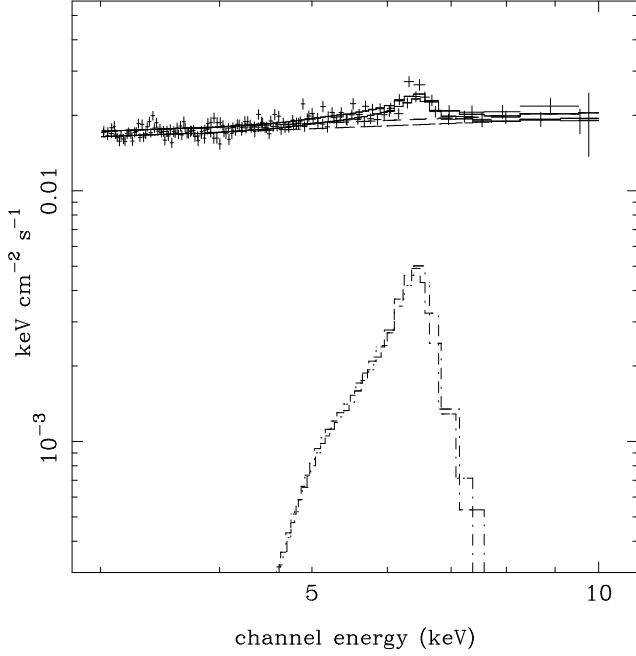


Figure 14. The continuum and the Fe K α line profile from the model `cloudfe` fitted to the *ASCA* data for MCG-6-30-15. Resulting parameter values are $r = 29.1$, $\Gamma = 1.856$. The remaining parameters were kept fixed: $\xi = 10^4$, $\theta_m = 90^\circ$, $\varpi = 0.1$.

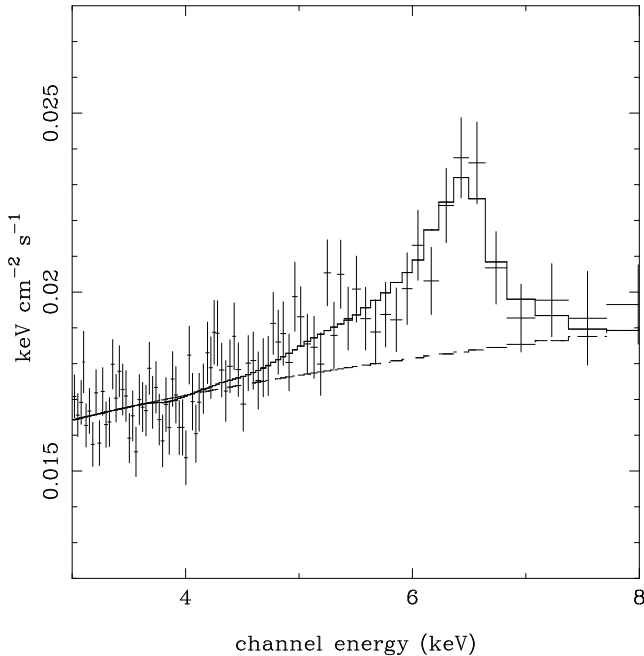


Figure 15. A detail of the line and the best fit profile are shown with better resolution between 4–8 keV.

alternative models (Fabian et al. 1995; Reynolds & Wilms 2000). However, in view of the complexity of the problem, it still seems somewhat premature to condemn other models as nonviable. We also remark that this object is probably somewhat exceptional case, though it is the best studied one at present.

We tested our model of the line profile predicted by the

clouds model by fitting it to the *ASCA* data from July 1994 (Tanaka, Inoue & Holt 1994; Fabian et al. 1994; Tanaka et al. 1995; Ebisawa et al. 1996). In order to avoid problems with modelling of the reflected component, the contribution from the warm absorber (Otani et al. 1996), and the cold absorption along the line of sight, we restrict our discussion to the SIS data in 3–10 keV band where the continuum can be represented roughly by a single power law. Since the detailed fitting is beyond the focus of the present work, we do not consider various luminosity states separately (instead, we follow the initial approach of Tanaka et al. 1995).

In order to have a reference for the results from our model we started by fitting the *ASCA* spectrum with a power law and a disc-line component (Fabian et al. 1989) from XSPEC (Arnaud 1996); see Table 1 for the results of χ^2 statistics. We assumed the line energy at 6.4 keV, consistently with the previous results. The X-ray incident flux was allowed to vary with the distance as $\propto r^{-\beta}$ with inner and outer disc radii fixed at $6 GM/c^2$ and $10^3 GM/c^2$ respectively. Then we compared those results with the fits to our model in two different parameter ranges.

3.3.1 The spherical configuration

First we consider the case of spherically symmetric arrangement of the clouds. The clouds cover the entire sphere ($\theta_m = 90^\circ$), so that the inclination angle is of no importance. Fitted parameters are: the photon index of the power law Γ , radius of the clouds distribution r , and the visibility factor ϖ defined as

$$\varpi = \frac{\omega}{\pi/2}. \quad (6)$$

Different versions of the model `cloudfe` were examined using XSPEC supplemented by three local model subroutines. They differ by corresponding values of ionization parameter:

- (i) an intrinsically narrow line in the rest frame of the clouds; this case refers to low ionization of the clouds surfaces where X-rays are reprocessed, $\xi \lesssim 10^2$;
- (ii) a broad line with $\xi = 10^3$ of the local emission;
- (iii) a broad line with $\xi = 10^4$ of the local emission.

The first of our models, with an intrinsically narrow line, does not provide adequate representation of the data. Strong residuals remain (as in the case of the Gaussian model), and the red wing cannot be reproduced successfully. However, for intrinsically broad line (with $10^3 \lesssim \xi \lesssim 10^4$) the red wing is formed locally as the result of Comptonization, and it has roughly the required shape. This model results in χ^2 comparable to the `diskline` profile (Tab. 1). The larger value of the ionization parameter gives marginally better fit than the lower one. Results of the fitting procedure with SIS0 and SIS1 detectors are shown in Figure 14. The line is reproduced with better resolution in Figure 15 (here we show only SIS0 data for clarity).

Our calculation imposes limits both on radius of the clouds distribution and on their covering factor. The former is constrained by requirement of appropriate location of the peak of the line; the gravitational shift has to balance somewhat increased energy of the line emission in this model (Fig. 6). The latter dependence reflects the fact that small radius of the clouds distribution goes in hand with

Table 1. Spectral fitting of the model parameters to the data for MCG–6–30–15. Standard χ^2 statistics was examined for different XSPEC models. The first two lines in the table refer to standard models for the sake of comparison (**diskline** and **powerlaw**), while the rest corresponds to the user supplemented model (**cloudfe**) as described in the text. The resulting values of three fitted parameters are given.

Model	ξ	Parameter #1	Parameter #2	Parameter #3	$\chi^2/\text{d.o.f.}$
diskline	—	$\Gamma = 1.810^{+0.019}_{-0.020}$	$\beta = -2.45^{+0.34}_{-0.30}$	$\theta_0 = 31.5^{+3.4}_{-3.2} \text{ deg}$	723.6/720
powerlaw	—	$\Gamma = 1.723^{+0.020}_{-0.021}$	—	—	852.5/722
cloudfe , spherical	10^2	$\Gamma = 1.728^{+0.021}_{-0.018}$	$r = 38^{+141}_{-37} \text{ GM}/c^2$	$\varpi = 0.52^{+0.29}_{-0.39} \text{ rad}$	804.1/720
cloudfe , spherical	10^3	$\Gamma = 1.792^{+0.024}_{-0.022}$	$r = 48.4^{+10.2}_{-6.3} \text{ GM}/c^2$	$\varpi < 0.19 \text{ rad}$	725.3/720
cloudfe , ring-type	10^3	$\Gamma = 1.796^{+0.025}_{-0.022}$	$r = 49.0^{+10.6}_{-7.1} \text{ GM}/c^2$	$\theta_m < 21.7 \text{ deg}$	724.9/720
cloudfe , spherical	10^4	$\Gamma = 1.856^{+0.029}_{-0.029}$	$r = 29.1^{+3.7}_{-4.3} \text{ GM}/c^2$	$\varpi < 0.13 \text{ rad}$	720.0/720
cloudfe , ring-type	10^4	$\Gamma = 1.857^{+0.026}_{-0.024}$	$r = 29.8^{+5}_{-4} \text{ GM}/c^2$	$\theta_m < 19.4 \text{ deg}$	721.6/720

dramatically strong smearing of the line, unless the effect of self-obscuration prevents us from having a direct view of the clouds with the highest velocities along the line of sight. We recall that the above discussion assumes Keplerian motion of the clouds; numerical values given in the column ϖ of Tab. 1 must be increased (less obscuration) if sub-Keplerian motion of the clouds is taken into account, as discussed in previous section.

3.3.2 The ring-type configuration

In order to see whether we can detract the strong requirements on the clouds obscuration at the expense of introducing partially flattened, ring-type geometry, we fitted the model assuming $\varpi = 0.5$ and varying θ_m . To illustrate the procedure, let us fix inclination angle at $\theta_0 = 30^\circ$, and consider two values of the ionization parameter, $\xi = 10^3$ and $\xi = 10^4$. The results are referred as ring-type models **cloudfe** in Tab. 1. The quality of the fits is comparable to those obtained for spherically symmetric case, however, the configuration comes out very flat, almost a ring indeed. We could not fit the data assuming $\varpi \rightarrow 1$ (the case of negligible obscuration) because such a flat distribution of the clouds clearly requires a substantial range of radii contributing to the spectrum (rather than a narrow ring). This conclusion is valid independently from the intrinsic broadening of the line due to internal Comptonization.

On the basis of several other attempts to find acceptable fits with different obscuration, we reached the conclusion that the currently available data is still not good enough to distinguish definitively in this model between a flat geometry and a spherically symmetric geometry of the accretion flow.

4 DISCUSSION

The effect of obscuration between the clouds plays an important role in the model: it restricts line-of-sight velocities of the clouds and suppresses the dependence of observed line profiles on inclination in comparison with the standard formulation of the disc-line model. Another interesting attribute of the clouds model is the requirement of high ionization of the material which is responsible for the iron-line emission: $\xi \gtrsim 10^3$. Such a high ionization has two consequences which we can briefly outline.

4.1 The role of high ionization

Since the red wing of the line is mostly due to Comptonization within the clouds surface layers (instead of kinematics of the accretion disc), the observed variability of the line profile must be also linked with the changes of the physical state of the clouds surfaces (Ebisawa et al. 1996; Lee et al. 1999). Self-consistent calculations of the resulting spectra present a difficult task because the thermal stability of the gas irradiated by hard X-ray photons depends on many factors at temperatures 10^5 – 10^6 K (Krolik 1999; Różańska 1999, and references therein). Even a minor change in the incident radiation may cause a dramatic response of the temperature and, consequently, the density of the irradiated gas through its expansion/contraction under constant pressure. Such fluctuations mean a significant change of the ionization parameter and of the intrinsic shape of the emitted line, without major alteration of the total luminosity of the source or the total flux in the iron line.

The demand of high ionization of the medium responsible for the line emission makes a difference from almost neutral environment of illuminated disc-type accretion flows, and there is hope to find its imprint also in the continuum. However, the limited spectral range of *ASCA* does not allow us to exploit such a possibility and to differentiate between the disc and the clouds models.

Also, we cannot presently distinguish the spherical configuration with strong self-obscuration of the clouds from the case of much flatter geometry and less obscuration. A better spectral resolution is needed in order to make the X-ray spectroscopy really a powerful tool and to determine the form of the accretion flow. Further work on the models is also needed to demonstrate true differences between the models.

4.2 The role of hydrostatic equilibrium

The calculations of local emissivity (Sect. 2.2) have been carried out under constant density approximation. If the clouds have enough time to achieve the hydrostatic equilibrium, the radiative transfer should be performed assuming constant pressure instead of constant density within the re-processing medium. Computations under the constant pressure assumption or, more generally, under the assumption of hydrostatic equilibrium show a specific temperature profile due to the radiative thermal instability at the intermedi-

ate temperatures (see e.g. Krolik, McKee & Tarter 1981; Róžańska & Czerny 1996; Róžańska 1999; Nayakshin et al. 1999). The irradiated medium is at the inverse-Compton temperature in the upper layers while being cold inside, with rather sharp transition determined by the effect of heat conduction (Róžańska 1999). Nayakshin et al. (1999) argue that the intermediate stable branch at the temperature about 10^6 K has a negligible influence on the formation of spectral features, while preliminary results of Monte Carlo simulations (Życki et al., in preparation) indicate that a possible enhancement of the iron abundance (crucial for the development of this branch; Lee et al. 1999) by a factor of ~ 2 may change this conclusion.

The problem remains unsettled for the moment, however, if the inverse-Compton temperature itself is low enough to allow for the formation of the $K\alpha$ line, then the line forms in a broad zone and the results of the computations do not depend crucially on the assumed density profile. This is quite possibly the case for the source MCG-6-30-15.

4.3 The role of inverse-Compton temperature

The spectral shape in the hard X-ray band was well determined for this object from the SAX data (Guainazzi et al. 1999). The best fit model gave the photon index $\Gamma = 2.04$ and the high-energy cut-off at 130 keV. The inverse-Compton temperature corresponding to such a spectrum is equal to 2.02×10^7 K, however, the soft photons emitted by the clouds and observed as the Big Blue Bump component reduce this value further.

The object is highly reddened in the optical/UV band. The extinction estimate based on the Balmer line indicates the $E(B-V)$ value in the range of 0.61–1.09 (Reynolds et al. 1997). Assuming a minimum value for the extinction these authors determine $L(\text{NIR}-\text{UV}) = 0.3 L(X)$. Somewhat larger values are favoured because too low bolometric luminosity of the internal source makes a large far-IR luminosity of this object difficult to explain. The upper limit on the extinction rises the flux at $\log(\nu) = 15$ by a factor of 12 in comparison with the lower limit. This fact together with an unconstrained high-frequency extension of the Big Blue Bump introduce significant uncertainty in the shape of the broad-band spectrum. Therefore, we can assume a standard shape of the spectrum, as in Abrassart & Czerny (2000), i.e. $L(\text{NIR}-\text{UV}) = 3 L(X)$. The observed ratio is slightly different from the intrinsic spectrum seen by the clouds (Abrassart & Czerny 2000; see their Eq. (12)). The correcting factor to this ratio is typically equal to 1.05–1.11. Assuming the value of 1.1 we finally obtain the Compton temperature of 4.7×10^6 K as a characteristic value for MCG-6-30-15.

The derived value falls just within the temperature range which resulted from our computations. The upper layer of the clouds, down to $\tau_{\text{es}} = 1$, has the temperature of 6.5×10^6 K assuming the parameter $\xi = 10^4$, and 1.8×10^6 K for $\xi = 10^3$. Therefore, in the case of the presented computations, the presence or the absence of hydrostatic equilibrium does not seem to pose a crucial question. This is quite fortunate because, under our present insufficient understanding of the clouds evolution, it is by no means clear which of the two approximations is more appropriate to the clouds that we consider – whether it is constant density or rather constant pressure assumption. Notice that for other Seyfert galaxies

than MCG-6-30-15 most probably their inverse-Compton temperatures will tend to be higher because their spectra are harder.

5 CONCLUSIONS

We presented a simple cloud model of AGN in which self-consistent computations of the intrinsic X-ray emission are supplemented by the phenomenological description of the clouds distribution. We demonstrated that satisfactory fits to the iron $K\alpha$ line feature can be obtained, and the model should be thus considered as viable and developed further, so that the phenomenological parameters are derived from the physical model of the clouds origin. We envisage the origin of the clouds due to erosion of the inner accretion disc. Detailed physics of the clouds formation remains beyond the scope of this paper but the adopted parameters (r , θ_0 , θ_m , ω) should reflect this scheme in a natural manner.

We remark that the scheme described in the present model is not restricted by recent considerations of Reynolds & Wilms (2000) because our model falls into that category of models in which the X-ray source is not viewed through the Comptonizing medium, and the clouds experience somewhat different continuum than the observer (Abrassart & Czerny 2000).

Observed profiles must be influenced by several other effects which were neglected in this paper due to our ignorance of the detailed model of the clouds properties. One can however anticipate the expected implications of a more refined model.

First, we ignored gravitational lensing for which one can expect a similar conclusion like for partial obscuration and sub-Keplerian motion of the clouds: the lensing effect enhances radiation coming from the clouds near the line of sight and on the remote side of the sphere. If included, the effect decreases the covering factor derived here by fitting the line profiles.

Second, we did not consider radial distribution of the clouds. This could be introduced in a straightforward manner but the assumption of almost constant radius provides a very good approximation in the current model. Hot parts of the clouds surfaces are those which lie innermost, where they are subject to strong primary irradiation by X-rays. The impact of the radial distribution can be absorbed in parameter ω (enhanced obscuration).

We conclude by emphasizing the fact that the present model differs from the disc-line model in the mechanism how the intrinsic spectrum is produced. There are however also common aspects of the two schemes. Indeed, a ring-like distribution of the clouds can be treated as a special case (small θ_m) resulting in profiles comparable to the disc-line model with appropriate emissivity. Notice, however, that here we obtained reasonable fits under the assumption of spherical or almost spherical clouds distribution. Certain degree of the flattening (characterized here by θ_m) is natural to this model where the clouds origin is in continuous erosion of the inner disc, but, on the other hand, θ_m cannot be too small because substantial Comptonization requires large covering factor. Finally, we remark that successful fits require strong gravitational field of the central body which shifts the line centroid towards lower energy.

ACKNOWLEDGEMENTS

The authors benefited from numerous discussions with Suzy Collin and Anne-Marie Dumont. They are grateful also to Piotr Źycki for help with the *ASCA* data, to Giorgio Matt for useful remarks about fitting the iron line, and to the referee for pointing out the question of hydrostatic equilibrium of the clouds and several other comments which helped us to improve our discussion. This research has made use of the TARTARUS database which is supported by Jane Turner and Kirpal Nandra under NASA grants NAG5-7385 and NAG5-7067. Part of this work was supported by the grant 2P03D01816 of the Polish State Committee for Scientific Research, and by Jumelage/CNRS No. 16 “Astronomie France/Pologne”. V.K. acknowledges hospitality of the Observatoire de Paris-Meudon, and partial support from the grants GAUK 63/98, GACR 202/98/0522 and 205/00/1685 in the Czech Republic.

REFERENCES

- Antonucci R., 1993, *ARA&A*, 31, 47
- Abrassart A., 2000a, in Proc. of the 32nd COSPAR Scientific Assembly (Nagoya 1998), *Advances in Space Research*, vol. 25, in press
- Abrassart A., 2000b, *A&A*, to be submitted
- Abrassart A., Czerny B., 2000, *A&A*, 356, 475
- Arnaud K. A., 1996, in *Astronomical Data Analysis Software and Systems V*, eds. G. Jacoby and J. Barnes, ASP Conference Series, vol. 101, p. 17
- Collin-Souffrin S., Czerny B., Dumont A.-M., Źycki P. T., 1996, *A&A*, 314, 393
- Cunningham C. T., Bardeen J. M., 1973, *ApJ*, 183, 273
- Czerny B., Zbyszewska M., Raine D., 1991, in *Iron Line Diagnostics in X-ray Sources*, ed. A. Treves (Berlin, Springer), p. 226
- Dabrowski Y., Fabian A. C., Iwasawa K., Lasenby A. N., Reynolds C. S., 1997, *MNRAS*, 288, L11
- Done C., Źycki P. T., 1999, *MNRAS*, 305, 457
- Dumont A.-M., Abrassart A., Collin S., 2000, *A&A*, in press
- Ebisawa K., Ueda Y., Inoue H., Tanaka Y., White N. E., 1996, *ApJ*, 467, 419
- Fabian A. C., Kunieda H., Inoue S., Matsuoka M. et al., 1994, *PASJ*, 46, L59
- Fabian A. C., Nandra K., Reynolds C. S., Brandt W. N. et al., 1995, *MNRAS*, 277, L11
- Fabian A. C., Rees M. J., Stella L., White N. E., 1989, *MNRAS*, 238, 729
- George I. M., Fabian A. C., 1991, *MNRAS*, 249, 352
- Gerbal D., Pelat D., 1981, *A&A*, 95, 18
- Guainazzi G., Matt G., Molendi S., Orr A. et al., 1999, *A&A*, 341, L27
- Iwasawa K., Fabian A. C., Reynolds C. S., Nandra K. et al., 1996, *MNRAS*, 282, 1038
- Krolik J. H., 1999, *Active Galactic Nuclei: From the Central Black Hole to the Galactic Environment* (Princeton, Princeton University Press)
- Krolik J. H., 1998, *ApJ Lett.*, 498, L13
- Krolik J. H., Madau P., Źycki P. T., 1994, *ApJ Lett.*, 420, L57
- Krolik J. H., McKee C. F., Tarter C. B. 1981, *ApJ*, 249, 422
- Laor A., 1991, *ApJ*, 376, 90
- Lee J. C., Fabian A. C., Brandt W. N., Reynolds C. S., Iwasawa K., 1999, *MNRAS*, 310, 937
- Martocchia A., Karas V., Matt G., 2000, *MNRAS*, 312, 817
- Matt G., Perola G. C., Stella L., 1993, *A&A*, 267, 643
- Misra R., Sutaria F. K., 1999, *ApJ*, 517, 661
- Muchotrzeb B., Paczyński B., 1982, *Acta Astron.*, 32, 1
- Nandra K., George I. M., Mushotzky R. F., Turner T. J., Yaqoob T., 1999, *ApJ Lett.*, 523, L17
- Nayakshin, S., Kazanas, D., Kallman, T. R., 1999, *ApJ*, submitted; astro-ph/9909359
- Netzer H., 1990, in *Active Galactic Nuclei*, eds. R. D. Blandford, H. Netzer, L. Woltjer (Berlin, Springer), p. 57
- Ohna E., Fukue J., Nakamura K. E., Mineshige S., 1995, *PASJ*, 47, 639
- Otani C., Kii T., Reynolds C. S., Fabian A. C. et al., 1996, *PASJ*, 48, 211
- Pariev V. I., Bromley B. C., 1998, *ApJ*, 508, 590
- Peterson B. M., 1997, *Active Galactic Nuclei* (Cambridge, Cambridge University Press)
- Reynolds C. S., Begelman M. C., 1997, *ApJ*, 488, 109
- Reynolds C. S., Fabian A. C., Nandra K., Inoue H. et al., 1995, *MNRAS*, 277, 901
- Reynolds C. S., Ward M. J., Fabian A. C., Celotti A., 1997, *MNRAS*, 291, 403
- Reynolds C. S., Wilms J., 2000, *ApJ*, 533, 821
- Rokaki E., Boisson C., 1999, *MNRAS*, 307, 41
- Róžańska A., 1999, *MNRAS*, 308, 751
- Róžańska A., Czerny B., 1996, *Acta Astronomica*, 46, 233
- Róžańska A., Dumont A.-M., Czerny B., Abrassart A., 2000, submitted
- Sulentic J. W., Marziani P., Calvani, M., 1998a, *ApJ Lett.*, 497, L65
- Sulentic J. W., Marziani P., Zwitter T., Calvani M., Dultzin-Hacyan D., 1998b, *ApJ*, 501, 54
- Tanaka Y., Inoue H., Holt S. S., 1994, *PASJ*, 46, L137
- Tanaka Y., Nandra K., Fabian A. C., Inoue H. et al., 1995, *Nature*, 375, 659
- Turner T. J., George I. M., Nandra K., Mushotzky R. F., 1998, *ApJ*, 493, 91
- Young A. J., Ross R. R., Fabian A. C., 1998, *MNRAS*, 300, L11
- Wang J.-X., Zhou Y.-Y., Wang T.-G., 1999, *ApJ Lett.*, 523, L129
- Weaver K. A., Reynolds C. S., 1998, *ApJ Lett.*, 503, L39
- Źycki P. T., Done C., Smith D. A., 1998, *ApJ Lett.*, 496, L25